Stoichiometry of Nucleotide Binding to Proteasome AAA+ ATPase Hexamer Established by Native Mass Spectrometry

Yadong Yu[1, 4], Haichuan Liu[2, 5], Zanlin Yu[1], H. Ewa Witkowska[2*], Yifan Cheng[1, 3*]

Supplemental Information

Examples of native MS studies on nucleotide-binding complexes.

Of note, several multimeric protein nucleotide-binding complexes have been analyzed by native MS, e.g., rotary V-type ATPases (1, 2) and proteasomes (3–7). Advances in MS mass resolution enabled studies focused on establishing nucleotide occupancy within the complex. For example, high accuracy and high reproducibility of molecular ion generation in separate experiments allowed for a differentiation between the ATP- and ADP-binding GroEL complexes (~800 kDa) utilizing Orbitrap (8) mass analyzer and resolved the stepwise addition of ATP to GroEL complex using QTOF (9) mass analyzer, thus allowing for probing allosteric mechanisms (10). Using modified Waters QTOF mass analyzer, simultaneous binding of ADP and the AMP-PNP ATP analogue (mass difference 79 Da) to the DNA mismatch repair MutS ABC ATPase was resolved for the ~200 kDa dimeric form of the complex (albeit not for its tetrameric counterpart) (11). Changes to the oligomeric state and nucleotide occupancy were demonstrated for the bacterial enhancer binding protein PspF AAA+ domain upon binding sigma factor σ54 (12). The study on the AAA+ ATPase p97 pointed to the presence of two distinct ADP and ATP-γS loading states suggesting cooperative nucleotide binding via discrete steps involving 5-6 nucleotides; interestingly, recombinant p97 that was purified in nucleotide-free buffer was reported to carry 10 ADP molecules (13).

Detection of over-charged oligomers in the native nanoESI MS of PAN proteins.

The highly charged molecular ion envelopes of PAN hexamers observed in the <D> and <T> regions as well as dimers seen in the <M> regions of the spectra (text Fig. 2 and 5) resemble protein molecular ions that are generated in the course of native MS via chemically or thermally induced supercharging (14–20) (21, 22). We refer to those ions as *over-charged* rather than supercharged to stress that they appeared in the absence of known supercharging-inducing conditions. We note that a similar phenomenon of generating both native-like and “extended-

like" structures was observed, albeit not discussed for octasome analysis that was performed using the same mass spectrometer that we have employed (Fig. 2) in Azegami et al. (23)

Despite the years of studies, the effects of supercharging on maintenance of native-like structures and protein ligand binding still remain intensely disputed in the literature (24–27). While we do not know what triggered formation of *over-charged* ions in our spectra, we compared their properties in terms of ligand binding capacity and levels of residual solvation to those of their native counterparts. We examined the results of four experiments in which high quality spectra of both native and *over-charged* hexamers were detected; we note that *over-charged* hexamers within the <T> m/z region were used for this analysis rather than their counterparts observed within the <D> region since the latter overlapped with the native dimers of much higher intensity. We found that *over-charged* species observed in our studies were consistent with the presence of bound ligands (Fig. S6A), suggesting a significant preservation of their higher order structure despite of them carrying "excessive" protons. The number of bound ADP nucleotides was found to be 5.7±0.22 and 5.9±0.24 for native and *over-charged* species, respectively. The residual solvation ratios for *over-charged* hexamers of PAN^{KA} vs PAN^{WT} were very close to those of native hexamers (1.11±0.07 and 0.98±0.06, respectively) (Fig. S6B). This result suggested that in accord with their native counterparts, the structures of *over-charged* ligand bearing PAN^{WT} and ligand-less PAN^{KA} ions were highly similar. Interestingly, the residual solvation ratios for *over-charged* vs. native species suggested the diminished level of residual solvation of the *over-charged* species (0.75±0.16 and 0.80±0.13 for both the PAN^{KA} and PAN^{WT} species, respectively (Fig. S6B).

The mechanism(s) of generation of the partially dissociated native-like species described in the main text and the *over-charged* "extended" multimeric structures have not been established in this study. Given the observed highly variable levels of the over-charged species along their

native-like counterparts, we hypothesize that their formation might have been triggered by small alterations in initial conditions of droplet generation (e.g., an uneven performance of an emitter), which in turn would affect – in a non-linear fashion – droplet evolution, ultimately leading to a variable level of degradation of a native-like hexameric structure leading to either dissociation and/or acquisition of excessive charging.

REFERENCES

1. Zhang, Z., Zheng, Y., Mazon, H., Milgrom, E., Kitagawa, N., Kish-Trier, E., Heck, A. J. R., Kane, P. M., and Wilkens, S. (2008) Structure of the yeast vacuolar ATPase. *J. Biol. Chem.* 283, 35983–35995

2. Zhou, M., Politis, A., Davies, R. B., Liko, I., Wu, K.-J., Stewart, A. G., Stock, D., and Robinson, C. V (2014) Ion mobility-mass spectrometry of a rotary ATPase reveals ATP-induced reduction in conformational flexibility. *Nat. Chem.* 6, 208–15

3. Loo, J. A., Berhane, B., Kaddis, C. S., Wooding, K. M., Xie, Y., Kaufman, S. L., and Chernushevich, I. V. (2005) Electrospray ionization mass spectrometry and ion mobility analysis of the 20S proteasome complex. *J. Am. Soc. Mass Spectrom.* 16, 998–1008

4. Sharon, M., Taverner, T., Ambroggio, X. I., Deshaies, R. J., and Robinson, C. V. (2006) Structural organization of the 19S proteasome lid: Insights from MS of intact complexes. *PLoS Biol.* 4, 1314–1323

5. Sharon, M., Witt, S., Felderer, K., Rockel, B., Baumeister, W., and Robinson, C. V. (2006)

20S proteasomes have the potential to keep substrates in store for continual degradation. *J. Biol. Chem.* 281, 9569–9575

6. Sharon, M., Witt, S., Glasmacher, E., Baumeister, W., and Robinson, C. V. (2007) Mass spectrometry reveals the missing links in the assembly pathway of the bacterial 20 S proteasome. *J. Biol. Chem.* 282, 18448–18457

7. Sakata, E., Stengel, F., Fukunaga, K., Zhou, M., Saeki, Y., Förster, F., Baumeister, W., Tanaka, K., and Robinson, C. V. (2011) The Catalytic Activity of Ubp6 Enhances Maturation of the Proteasomal Regulatory Particle. *Mol. Cell* 42, 637–649

8. Rose, R. J., Damoc, E., Denisov, E., Makarov, A., and Heck, A. J. R. (2012) High-sensitivity Orbitrap mass analysis of intact macromolecular assemblies. *Nat. Methods* 9, 1084–6

9. Dyachenko, A., Gruber, R., Shimon, L., Horovitz, A., and Sharon, M. (2013) Allosteric mechanisms can be distinguished using structural mass spectrometry. *Proc. Natl. Acad. Sci. U. S. A.* 110, 7235–9

10. Sharon, M., and Horovitz, A. (2015) Probing allosteric mechanisms using native mass spectrometry. *Curr. Opin. Struct. Biol.* 34, 7–16

11. Monti, M. C., Cohen, S. X., Fish, A., Winterwerp, H. H. K., Barendregt, A., Friedhoff, P., Perrakis, A., Heck, A. J. R., Sixma, T. K., Van Den Heuvel, R. H. H., and Lebbink, J. H. G. (2011) Native mass spectrometry provides direct evidence for DNA mismatch-induced regulation of asymmetric nucleotide binding in mismatch repair protein MutS. *Nucleic Acids Res.* 39, 8052–8064

12. Zhang, N., Gordiyenko, Y., Joly, N., Lawton, E., Robinson, C. V., and Buck, M. (2014) Subunit dynamics and nucleotide-dependent asymmetry of an AAA+ transcription complex. *J. Mol. Biol.* 426, 71–83

13. Schuller, J. M., Beck, F., Lössl, P., Heck, A. J. R., and Förster, F. (2016) Nucleotide-dependent conformational changes of the AAA+ ATPase p97 revisited. *FEBS Lett.* 590, 595–604

14. Lomeli, S. H., Yin, S., Ogorzalek Loo, R. R., and Loo, J. A. (2009) Increasing Charge While Preserving Noncovalent Protein Complexes for ESI-MS. *J. Am. Soc. Mass Spectrom.* 20, 593–596

15. Iavarone, A. T., Jurchen, J. C., and Williams, E. R. (2001) Supercharged Protein and Peptide Ions Formed by Electrospray Ionization. *Anal Chem* 73, 1455–1460

16. Sterling, H. J., and Williams, E. R. (2009) Origin of Supercharging in Electrospray Ionization of Noncovalent Complexes from Aqueous Solution. *J. Am. Soc. Mass Spectrom.* 20, 1933–1943

17. Teo, C. A., and Donald, W. A. (2014) Solution additives for supercharging proteins beyond the theoretical maximum proton-transfer limit in electrospray ionization mass spectrometry. *Anal. Chem.* 86, 4455–4462

18. Chingin, K., Xu, N., and Chen, H. (2014) Soft supercharging of biomolecular ions in electrospray ionization mass spectrometry. *J. Am. Soc. Mass Spectrom.* 25, 928–934

19. Ogorzalek Loo, R. R., Lakshmanan, R., and Loo, J. A. (2014) What protein charging (and

supercharging) reveal about the mechanism of electrospray ionization. *J. Am. Soc. Mass Spectrom.* 25, 1675–1693

20. Martin, L. M., and Konermann, L. (2020) Enhancing protein electrospray charge states by multivalent metal ions: Mechanistic insights from MD simulations and mass spectrometry experiments. *J. Am. Soc. Mass Spectrom.* 31, 25–33

21. Khristenko, N., Amato, J., Livet, S., Pagano, B., Randazzo, A., and Gabelica, V. (2019) Native ion mobility mass spectrometry: When gas-phase ion structures depend on the electrospray charging process. *J. Am. Soc. Mass Spectrom.* 30, 1069–1081

22. Konermann, L., Metwally, H., Duez, Q., and Peters, I. (2019) Charging and supercharging of proteins for mass spectrometry: Recent insights into the mechanisms of electrospray ionization. *Analyst* 144, 6157–6171

23. Azegami, N., Saikusa, K., Todokoro, Y., Nagadoi, A., Kurumizaka, H., Nishimura, Y., and Akashi, S. (2013) Conclusive evidence of the reconstituted hexasome proven by native mass spectrometry. *Biochemistry* 52, 5155–5157

24. Hogan, C. J. J., Ogorzalek Loo, R. R., Loo, J. A., de La Mora, F., Hogan Jr, C. J., Ogorzalek Loo, R. R., Loo, J. A., and Mora, J. F. de la (2010) Ion mobility-mass spectrometry of phosphorylast B ions generated with supercharging reagents but in charge-reducing buffer. *Phys. Chem. Chem. Phys.* 12, 13476–13483

25. Sterling, H. J., Kintzer, A. F., Feld, G. K., Cassou, C. A., Krantz, B. A., Williams, E. R., and Bryan, A. (2011) Supercharging Protein Complexes from Aqueous Solution Disrupts their Native Conformations Conformations. *J Am Soc Mass Spectrom* 23, 191–200

26. Yao, Y., Richards, M. R., Kitova, E. N., and Klassen, J. S. (2016) Influence of Sulfolane on ESI-MS Measurements of Protein-Ligand Affinities. *J. Am. Soc. Mass Spectrom.* 27, 498–506

27. Going, C. C., Xia, Z., and Williams, E. R. (2016) Real-time HD Exchange Kinetics of Proteins from Buffered Aqueous Solution with Electrothermal Supercharging and Top-Down Tandem Mass Spectrometry. *J. Am. Soc. Mass Spectrom.* 27, 1019–1027

Supplemental Figures with Legends

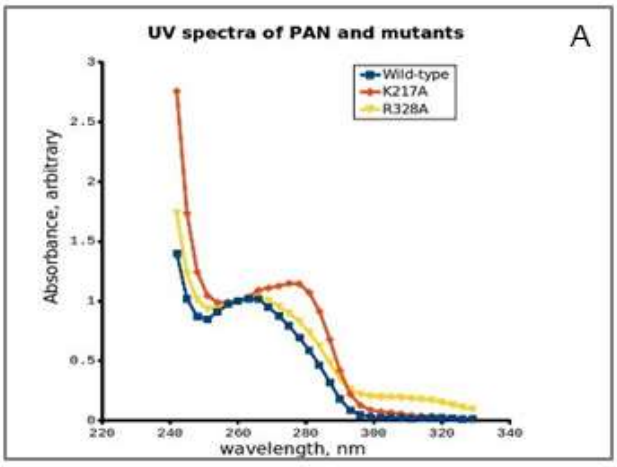

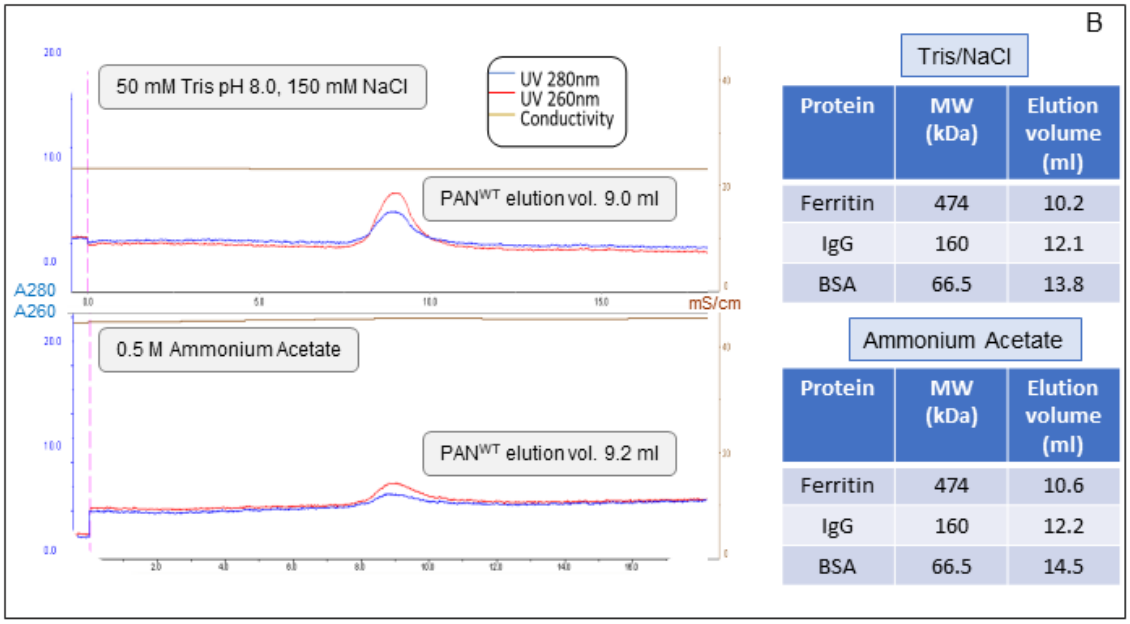

Tris/NaCl

Protein	MW (kDa)	Elution volume (ml)
Ferritin	474	10.2
IgG	160	12.1
BSA	66.5	13.8

Ammonium Acetate

Protein	MW (kDa)	Elution volume (ml)
Ferritin	474	10.6
IgG	160	12.2
BSA	66.5	14.5

Fig. S1 AB. Evaluation of integrity of PAN preparations. **A:** UV spectra of PAN proteins. PAN^{WT}, PAN^{KA}, and PAN^{R328A} are shown in blue, orange and yellow, respectively. PAN^{WT} and PAN^{R328A} show higher A260 than A280 whereas PAN^{KA} shows the opposite relationship, indicating nucleotide content in the first two but none in PAN^{KA}. **B:** Gel filtration analysis of PAN^{WT}. Gel filtration elution profiles of **P**AN^{WT} in Tris/NaCl (top) and 0.5 M ammonium acetate (bottom) buffers using Superdex 200 10/300 column are shown. Both PAN and standard proteins eluted slightly faster in the Tris buffer.

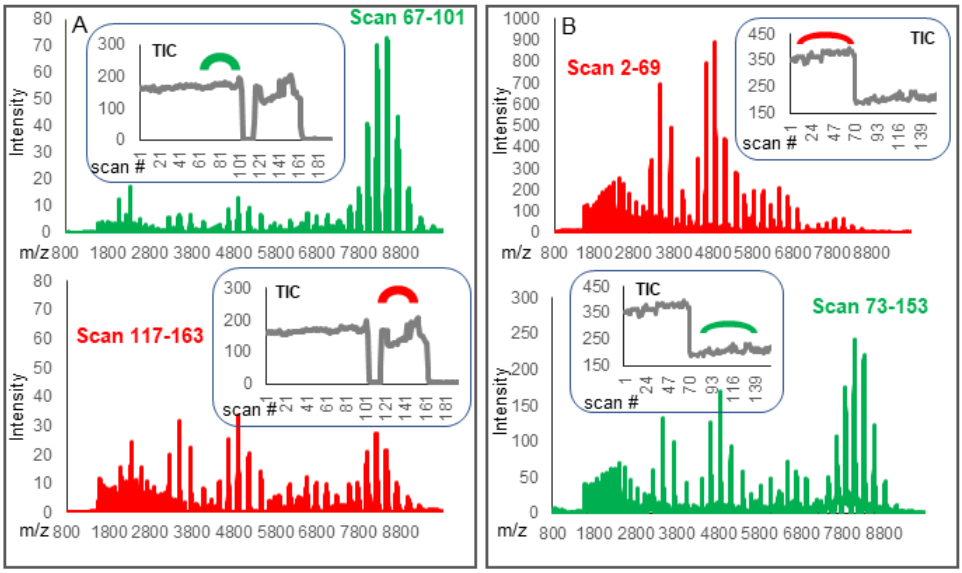

Fig. S2AB. **Examples of fluctuations in the extent of PAN hexamer dissociation observed during a single nanoESI MS acquisition.** Panels A and B respectively show Massign-processed spectra of PAN^{WT} and PAN^{KA}, which were derived by summing up the scans that were marked at the total ion current (TIC) traces in the insets. Data showing low and high level of hexamer dissociation are shown in green and red, respectively.

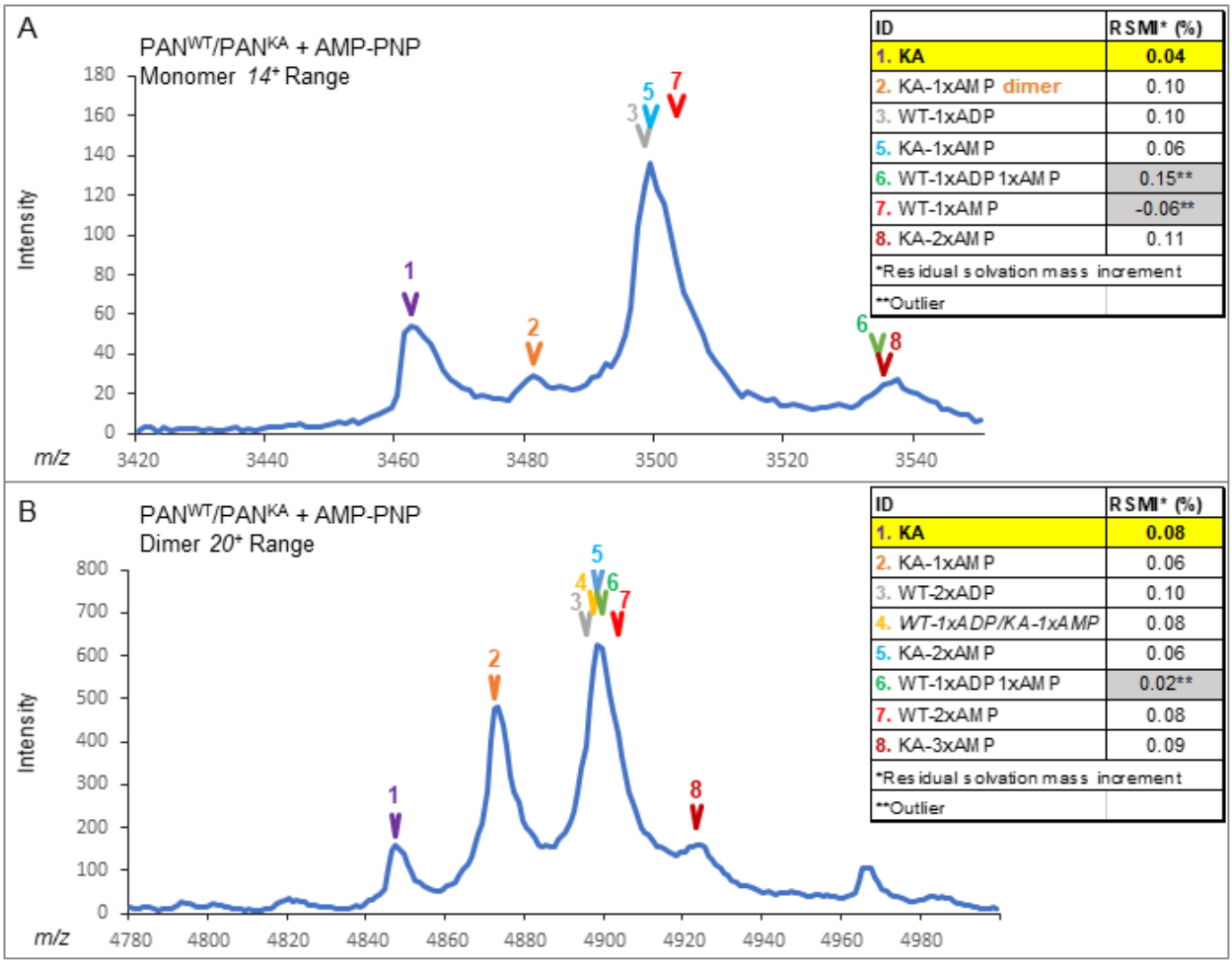

Fig. S3AB. Evaluation of the native monomer *14+* (panel A) and native dimer *20+* (panel B) regions of the spectrum of the mixture of PAN^{WT} and PAN^{KA} following nucleotide exchange with AMP-PNP. Potential components of the sample carrying ADP and/or AMP-PNP are listed in the inset tables and marked in the spectra. The tables provide values for residual solvation mass increment (RSMI) for monomers and dimers calculated for various nucleotide compositions using experimental masses of peaks with which they potentially are associated. The RSMI values of apo PAN^{KA} monomer and dimer are provided for comparison and compositions that are associated with RSMI values that differ from those of apo PAN^{KA} by factor of 4 or more are annotated as outliers. The potential composition of a mixed dimer of WT-ADP and KA-AMP-PNP is italicized, as this type of hybrid products of PAN hexamer dissociation were never observed in our studies. As it is clear from the spectra, reliable differentiation between potential candidate species 3-7 is not feasible at the resolution that was achieved in this study.

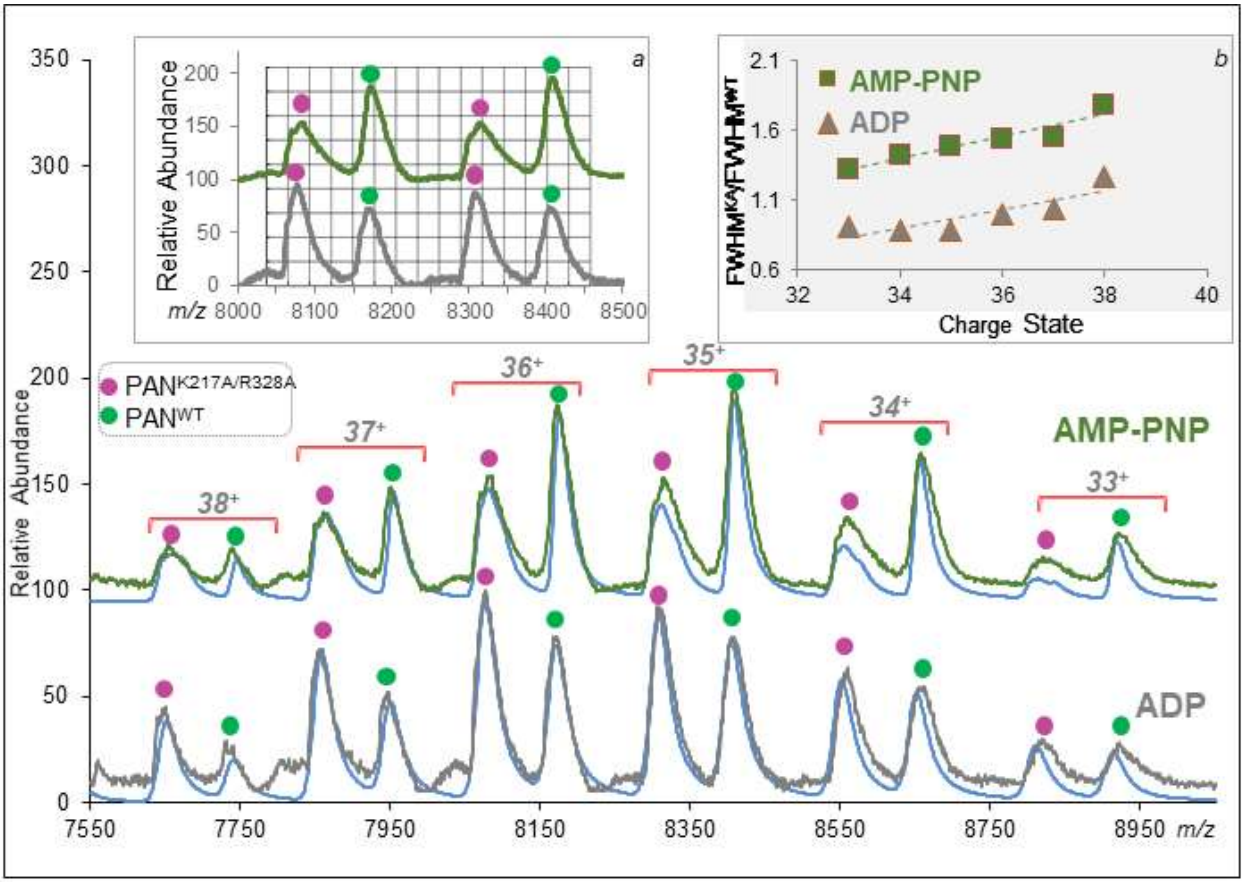

Fig. S4. **Analysis of the PAN^{WT} and a double mutant PAN$^{K217A/R328A}$ mixture following ligand exchange with AMP-PNP.** Dark grey and green graphs show Massign-processed experimental spectra of a hexamer region (<H>) of a mixture of PAN$^{K217A/R328A}$ with PAN^{WT} in its ADP- (bottom) and AMP-PNP-binding (top) forms, respectively. Blue lines show the sum of Massign simulated spectra of component hexamers. Data for three MS analyses were combined. While multiple PAN$^{K217A/R328A}$ -AMP-PNP binding protein forms are not resolved here, their presence is inferred by comparing peak width (FHWM) of this mutant with and without a bound AMP-PNP (showed in more detail in inset a). The peaks of PAN$^{K217A/R328A}$ in the presence of AMP-PNP former are much broader: FHWM^{KARA}/FHWM^{WT} was1.0±0.14 and 1.5±0.15 in the absence and presence of AMP-PNP (T-test=1.49E-04), respectively (inset b).

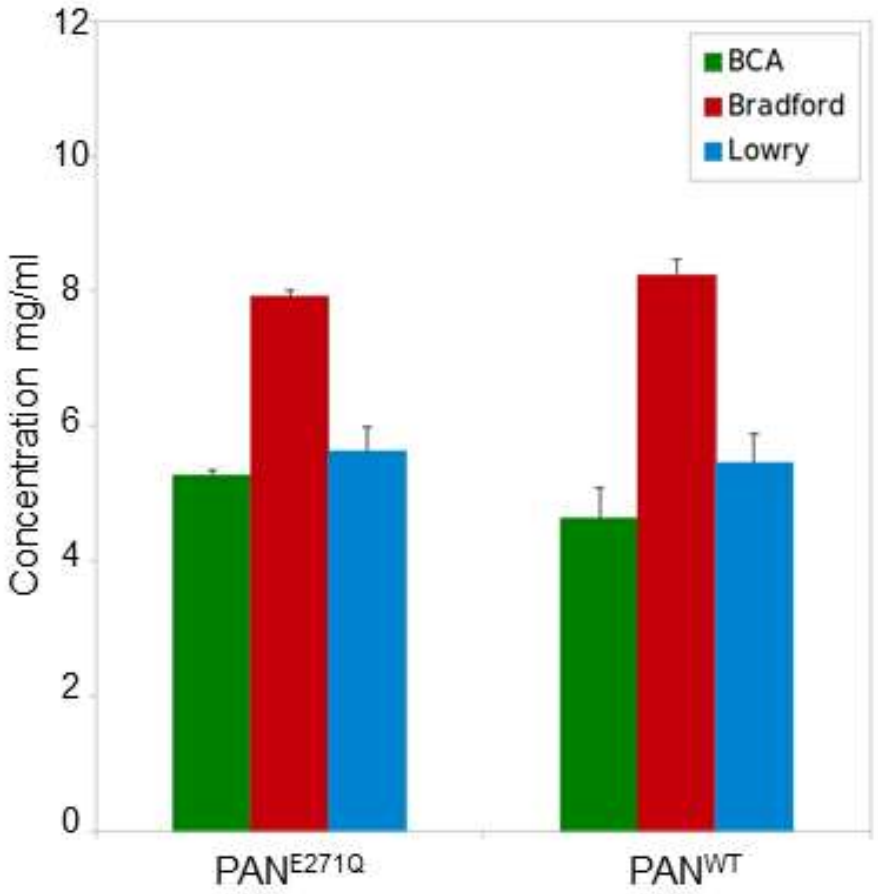

Fig. S5. Comparison of protein concentration measurement using three different commercially available assay kits. WT PAN and Walker B mutant (PAN E271Q) were analyzed. The results of 3 experiments are shown.

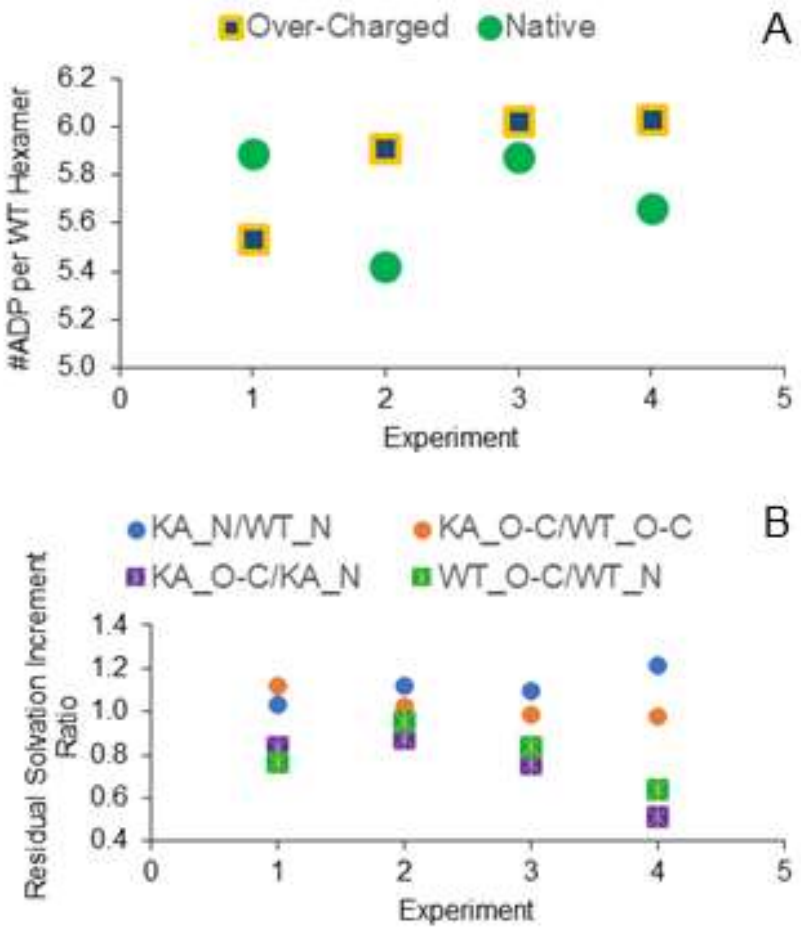

Fig. S6 AB. Comparison of native and *over-charged* PAN hexamers. A: *Over-charged* PAN^{WT} hexamers carry ADP. ADP binding to PAN^{WT} derived from the native and *over-charged* hexamer data observed within m/z mass ranges <H> and <T>, respectively. The results of 4 independent analyses of PAN^{WT}+PAN^{KA} mixtures are shown. The number of bound ADP nucleotides was found to be 5.7±0.22 and 5.9±0.24 for native and *over-charged* species, respectively. **B:** Comparison of residual solvation mass increments for WT to KA PAN hexamers in their native and *over-charged* states. Native and *over-charged* species for each KA and WT protein are annotated with "_N" and "_O-C", respectively. Residual solvation mass increment ratios for KA vs WT PAN species were similar for both native and *over-charged* forms (i.e., 1.11±0.07 and 1.03±0.06, respectively, marked with light blue and orange dots). For both, WT and KA PAN, residual solvation was significantly lower for the *over-charged* species in comparison to their native counterparts, i.e., over-charged to native ratios were 0.75±0.16 and 0.80±0.13 for KA and WT proteins, respectively (annotated with green and purple crossed squares).